A mathematical framework for evaluation of column shape profiles for an Advanced Gas-cooled Reactor core model subject to seismic excitation

R.E.White[1], T. Gokce[1], O. Oddbjornsson[2], K.Bourne[1], A. J. Crewe[1,*], L. Dihoru[1], T. Horseman[1], M. Dietz[1], P. Kloukinas[3], C.A. Taylor[1]

[1] Earthquake and Geotechnical Engineering Group, Faculty of Engineering, University of Bristol, University Walk, Bristol BS8 1TR, UK; rory.white@bristol.ac.uk ; tansu.gokce@bristol.ac.uk; k.bourne@bristol.ac.uk; luiza.dihoru@bristol.ac.uk; tony.horseman@bristol.ac.uk; m.dietz@bristol.ac.uk; colin.taylor@bristol.ac.uk

[2] EFLA Consulting Engineers, Lynghals 4, 110 Reykjavik, Iceland; Olafur.oddbjornsson@efla.is

[3] Department of Civil Engineering, School of Engineering, University of Greenwich, Central Avenue, Chatham Maritime, Kent ME4 4TB, UK, P.Kloukinas@grerenwich.ac.uk

* Corresponding Author: A.J.Crewe@bristol.ac.uk

Abstract

The safe shutdown of Advanced Gas-cooled Reactor (AGR) nuclear power stations in response to a seismic event is vital to their safety case. The tubular graphite bricks used to moderate the neutrons within an AGR core are arranged in columns whose bores provide channels for either fuel or control rods. Earthquake-induced distortion of the channels could impede the insertion of the control rods and compromise the safe shut-down, maintenance and servicing of the reactor. This paper presents a mathematical framework, utilising Euler mechanics, to evaluate the column shape displacement profiles of fuel and control rod channels within a state-of-the-art quarter-sized physical model of an AGR core when subjected to seismic loading. The data obtained from sensors installed within the model bricks, and configured to monitor interface displacements, are used to infer the global behaviour of a multi-stacked brick column subject to seismic excitation. Directly measured displacements of the top of the brick columns, obtained using a motion capture vision system, are compared with the displacements calculated using the framework presented, verifying the validity of the procedure. Statistical analysis is employed to quantify and characterise the performance of the Euler mechanics method. For multiple model build configurations, which represent different brick-cracking scenarios in an aged core, the Pearson correlation factor between the direct and indirect measurements is evaluated for the top of the column displacements giving an average value of 0.96 in the direction of the input motion. This shows that good agreement is achieved for the column shape displacement time-histories. The seismic responses are shown to be significantly larger in amplitude in the presence of large numbers of cracked bricks.

Keywords: Advanced gas cooled reactor; displacement analysis; stacked column; column shape displacement; seismic testing

1. Introduction

In 2020 nuclear power generated 16% (8.1GW) of the UKs electricity (Department for Business, Energy & Industrial Strategy and Nuclear Decommissioning Authority, 2021), 31% of that supplied from low-carbon sources. Most of this capacity came from an aging fleet of fourteen Advanced Gas-cooled Reactors (AGRs) that were commissioned across six UK sites between 1976 and 1988. Utilising graphite for neutron moderation and carbon dioxide for cooling, AGRs resembled the first-generation of (Magnox) British nuclear reactors but were designed to offer an enhanced economic performance. Within AGR cores, the graphite has the form of an array of interlocked tubular bricks. Stacked in columns, the bores of the bricks create channels for the transport of fuel, control rods and coolant. Safe operation requires that transport remains unimpeded, regardless of the imposed environmental demand. Seismic load must be accounted for, and current standards require that nuclear plant should be resilient to at least 0.1 g peak ground acceleration (PGA), while AGR operators require safe shutdown capability via control-rod insertion in the event of a more severe earthquake (probability of exceedance of 10^{-4} per annum).

AGRs are now at or beyond their design life (Bonivento et al., 2008 and Young et al., 2019). Since commissioning the ongoing effects of fast neutron irradiation and radiolytic oxidation within AGR cores have resulted in aging of the graphite components resulting in variation to the physical and mechanical properties. These include changes to geometry and strength, and an increase in the potential for differential shrinkage-induced cracking (Neighbour, 2007) (i.e., cracking that occurs when the inner and the outer areas of a tubular brick shrink at different rates). The continued safe operation of AGRs relies on a robust understanding of core behaviour to be established accounting for both actual and anticipated future states and achieved through numerical (Jones, 2007; Kralj et al., 2005; McLachlan et al., 2007) and physical modelling.

The earliest physical model for assessing the seismic behaviour of AGR core-like structures was developed by the National Nuclear Corporation in 1985 (Rogers, 2012) and comprised a simple 9×9×1 tall brick array. AMEC ltd modelled a greater number of bricks but at smaller scale ($1/8^{th}$) to investigate potential fuel channel displacements (Castro, 2005). Several enhanced analytical methods and physical models for static and dynamic behaviour have been reported in the last decade (Flewitt and Wickham, 2015; Neighbour, 2013). Between 2008 and 2012, a quarter-sized near-full single layer 20-rings array model was developed at the University of Bristol (Dihoru et al, 2015, 2011). Known as the Single-Layer Array (SLA), the model enabled exploration of the basic mechanics of the core system as a precursor for a more sophisticated modelling tool, called the Multi-Layer Array (MLA). The MLA is a quarter-sized AGR-core like structure consisting of 8 layers of 20 bricks arranged to match the octagonal layout of an AGR core (Dihoru, 2017). Significant experimental testing, modelling and analysis has been employed over the past decade on the MLA core model (Dihoru et al., 2020, 2019, 2018; Voyagaki et al., 2018). For this testing the MLA model (Figure 1) was mounted onto the shaking table at the University of Bristol and subjected to a range of seismic and harmonic input motions to investigate the response of the array to different seismic events. This work enabled the validation of numerical models for predicting the behaviour of AGR cores when subjected to various input motions with varying amplitude and direction.

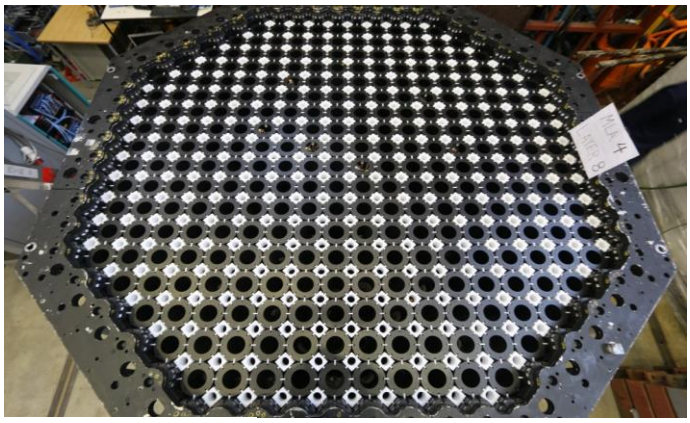

Fig. 1. Plan view of the MLA showing the top layer of bricks.

The fundamental challenge for this research was to understand the constrained rocking response of multibody graphite column arrays connected by a shear inducing keying system in a polygonal configuration (Voyagaki et al., 2018). Details of the MLA build configuration, components, keying system and rocking features can be found in Dihoru et al. (2017). The classical problem of rocking response involves a rigid body resting on a horizontal plane, subjected to horizontal dynamic excitation. Although apparently simple, it is a highly complex nonlinear problem that has been the subject of extensive research, both theoretical (Bachman et al., 2019; Dimitrakopoulos and DeJong, 2012a, 2012b; Kounadis, 2013; Psycharis et al., 2013; Reggiani Manzo and Vassiliou, 2021, 2019; Voyagaki et al., 2015, 2014, 2013; Zhang and Makris, 2001) and experimental (Anooshehpoor, 2004; Peña et al., 2007; Vassiliou et al., 2021). The case of multibody rocking and sliding is significantly more complex and is still not adequately understood, despite a considerable number of research efforts mostly related to earthquake stability of multidrum classical columns (Dasiou, 2009; Konstantinidis and Makris, 2005; Mouzakis et al., 2002; Papantonopoulos et al., 2002; Psycharis et al., 2003, 2000). In these studies of single-body and multibody rocking, the blocks are allowed to overturn, and thus, the systems investigated are inherently unstable. Stability in the classical sense of overturning is not an issue in the graphite core (MLA) case, as the rocking blocks are restricted by a combination of the shear keys and the lateral boundary of the reactor (Dihoru et al., 2017). This collection of rigid blocks could, therefore, be better characterised as a special type of self-centring structural system, with its dynamic response during rocking being the focus, as opposed to overturning. Of particular interest are the deformations of the core, the separations of the bricks during shaking, and the occurrence and extent of component disengagement, when keys separate causing brick detachment and large dynamic movements, particularly when the core is degraded and components have cracked. The latter issues may have safety implications during a seismic event, as severe permanent distortion of the vertical channel profiles caused by key disengagement or cracked components could block the insertion of the control rods and prevent the safe shutdown of the reactor. It is worth mentioning that this is never the case for the intact array, as its design inherently avoids the issues that might arise when component cracking is involved. It is possible that graphite bricks may potentially crack during an earthquake allowing keys to disengage forthwith. Nevertheless, examining the dynamics of the intact MLA is fundamental for understanding the physics of the larger problem.

During testing, the seismically induced motions of bricks within the MLA are monitored using a variety of embedded sensors (Dihoru et al., 2017). In addition, the motion of the top of the brick columns

are monitored using motion capture infrared vision tracking and high resolution camera systems (Dihoru et al., 2019). Displacements of measured interfaces and brick column tops are crucial in evaluating the full dynamic response of a stacked column housed within the MLA core model. Measurement techniques and displacement characterisation of stacked fuel brick, referred to herein as lattice bricks, column interface data is outlined in Dihoru et al. (2021) demonstrating the applicability of neural network modelling to extract vertical and rotational motion. However, it is apparent that significant training from a significantly wide source of measurements is required to ensure that a sufficiently robust neural network is developed. For classification of keyed- and unkeyed-interstitial bricks, referred to herein as interstitial and filler bricks respectively, displacement measurements have been calculated using the nonlinear system identification method applied to each brick interface, as described in Oddbjornsson et al. (2021). This method allowed direct extraction of six degree-of-freedom (DoF) displacements representing the full translational and rotational movement of an adjacent pair of vertically stacked interstitial and filler bricks. This paper extends work done by these previous studies, using the individual column interface measurements to formulate the global column shape displacement profile. This allows the complete behaviour of an instrumented stacked column to be characterised directly from experimental measurements permitting the implicit evaluation of the column shape profile.

This paper presents a mathematical framework for the indirect evaluation of the column shape displacement profiles of an instrumented brick column within the MLA. Data acquired from both lattice and interstitial stacked brick column interfaces are processed and converted into a global frame of reference. A variety of experimental MLA build configurations are investigated to assess the validity of the indirect column shape displacement algorithm for both instrumented interstitial and lattice stacked brick columns. The influence of cracked brick arrays on the resulting dynamic column shape profiles is also explored. The evaluated column shape results are compared with direct measurements of movement tracking from an infrared vision system (Dihoru et al., 2019, 2017) to assess the validity of this mathematical approach. A comprehensive statistical and error analysis is performed to quantify the performance of the proposed procedure with the associated deviations and uncertainty. This analysis procedure is not limited to this specific civil/nuclear engineering application but can be applied to generic stacked columns with measurements at each layer and interface. This study aims to answer the following research questions: (i) is it possible to indirectly evaluate the global column shape behaviour, based on displacement, of instrumented columns from brick interface measurements housed within a model AGR core and (ii) how does the Euler mechanics based method perform compared to the directly measured top of column trajectories.

2. MLA Layout and Instrumentation

The MLA (Figure 1) comprises eight layers representing the inner 10 octagonal rings of an AGR core. It has a plan size of 2.497m x 2.497m and a height of 1.731m. The components located on the bottom layer and outer ring of the MLA are connected to the MLA frame, and as a result their motion relative the shaking table is constrained. The MLA frame is a seismically rigid restraining frame that laterally envelopes the array. It is the inner nine rings and top seven layers which are considered ‘active’ locations within the MLA. Each column of the MLA is constructed from quarter-sized models of the graphite moderator bricks within an AGR core. The graphite moderator brick types include keyed interstitial bricks, unkeyed interstitial bricks and fuel bricks. Neighbour (2007) provides a detailed description of all components with an AGR core. For the purposes of the MLA experiments, the model

keyed interstitial bricks are referred to as interstitial bricks, the model unkeyed interstitial bricks are referred to as filler bricks and the model fuel bricks are referred to as lattice bricks. The lattice bricks are stacked to form columns of lattice bricks, each comprising eight bricks. The top brick of the lattice brick column is two-thirds the full brick height to ensure that the top level of the array is flat and aligned with the top brick of the interstitial columns. The interstitial and filler bricks are alternately stacked to form the interstitial columns, comprising seven interstitial bricks and six filler bricks. Figure 2 presents the plan view of the MLA, a detail of the lattice and interstitial columns, and brick and interface labels within a single column of lattice and interstitial bricks respectively. The geometry of the interstitial and filler bricks is provided in Figure 3(a&b), and Figure 3(c&d) presents the lattice brick dimensions.

All but the first MLA layout also included 'cracked' lattice bricks that were installed at various locations throughout the active layers of the array. Referred to as Doubly, Triply and Quadruply Cracked Bricks (DCBs, TCBs and QCBs), these components model instances within an AGR core where moderator bricks degrade with age and become cracked (Neighbour, 2007; Jones, 2005). A DCB and an instrumented version of a DCB (IDCB) are presented in Figure 3(e&f) whilst an example of a TCB and a QCB are shown in Figure 3(g&h).

2.1. Data acquisition system and sensors

The instrumented columns make use of a micro-Data Acquisition System (μDAQ) that was designed specifically for the MLA (Crewe et al. 2018). It was critical that the measurement system did not interfere with the dynamic response of the bricks, therefore the connections associated with both the sensors themselves and the storage of the sensor data had to be minimised. To this end the μDAQ boards were housed within the lattice and filler bricks to enable local storage of sensor data.

Measurement of the displacement between the interstitial and filler bricks was undertaken using bi-axial Hall Effect sensors, as described by Oddbjornsson et al. (2021). A custom calibration procedure, also detailed in Oddbjornsson et al. (2021) enabled the 12 individual data channels to be converted to accurate measurements of motion in all six degrees of freedom. Each instrumented interstitial column comprised 13 interface measurements. The lattice brick columns were instrumented with four vertical spring-loaded Linear Conductive Potentiometers (LCPs) that enabled four single degree of freedom vertical displacement measurements to be captured at seven of the eight column interfaces. Refer to Figure 2 for the location of each instrumented interface. The LCPs were dynamically calibrated using sinusoidal inputs to ensure that the vertical displacement at each column interface was accurately recorded. Qualysis™ motion capture software was employed for displacement tracking of the MLA frame, and of the top layer bricks on the instrumented lattice and interstitial columns. The Qualysis™ vision system made use of five infrared (IR) cameras, whose installed location was chosen to ensure that the system could achieve robust tracking of the IR markers during dynamic testing. Seven markers were uniformly distributed around the MLA frame, and three markers were installed on the top brick of each instrumented column. The use of multiple markers at each measurement point ensured that suitably accurate tracking could be achieved for each component. This allowed the evaluation of a mean marker trajectory per component. Tracking the motion of both the restraint frame and the top layer bricks of each instrumented column enabled relative displacement to be investigated. The displacement data for the top layer bricks, measured using the vision system, could then be directly compared to the column displacement calculated using the μDAQ data.

The shaking table input acceleration motion was tracked using seven uni-axial Setra 141a accelerometers (S) that were mounted on the top surface of the shaking table to give the table motion in six degrees of freedom. The direction and location of the accelerometers are given in Figure 2. For a typical single axis test e.g. a 0.4g HPB motion in the x direction, the maximum shaking table displacement was 14mm in x direction and less than 0.2mm in Y and Z directions. The maximum rotational displacements measured were less than 0.02° for roll, pitch and yaw. The motion capture, μDAQ and Setra sensor systems were time-synchronised using an external clock system which is described in full by Voyagaki et al. (2018). The data from the LCP and Hall effect sensors was acquired by the μDAQ system at a rate of 5000Hz. The Setra accelerometer data was also acquired at 5000Hz, whilst the vision system was sampled at 200Hz. During the acquisition of the μDAQ and Setra measurements, an eighth order anti-aliasing Butterworth filter with a cut-off frequency of 1400Hz was implemented. The application of the anti-aliasing filter induced a time-lag between the μDAQ/Setra data and the motion capture vision system that was quantified as 0.05s from initiation, which equated to 5 samples at the 5000Hz sampling rate. This discrepancy was accounted for during post-processing. The μDAQ and Setra data were down sampled and decimated to the vision system's sampling frequency of 200Hz for data processing and analysis. Finally, a sixteenth order low-pass zero-phase Butterworth filter with a cut-off frequency of 80Hz was applied to μDAQ displacement measurements, acquired from the LCP and Hall effect sensors, to mitigate any high-frequency noise effects.

It was not feasible to instrument the entire array due to both practical and resourcing constraints, so the position of the instrumented columns was carefully chosen for each experiment to focus on areas of interest. Up to six lattice columns and eight interstitial columns could be instrumented per experiment. For each instrumented column, data was recorded at the brick interfaces, be this a lattice/lattice brick interface or an interstitial/filler brick interface. Both the interface naming convention (prefixed by 'J'), and the brick numbering convention is based on the layer number as detailed in Figure 2.

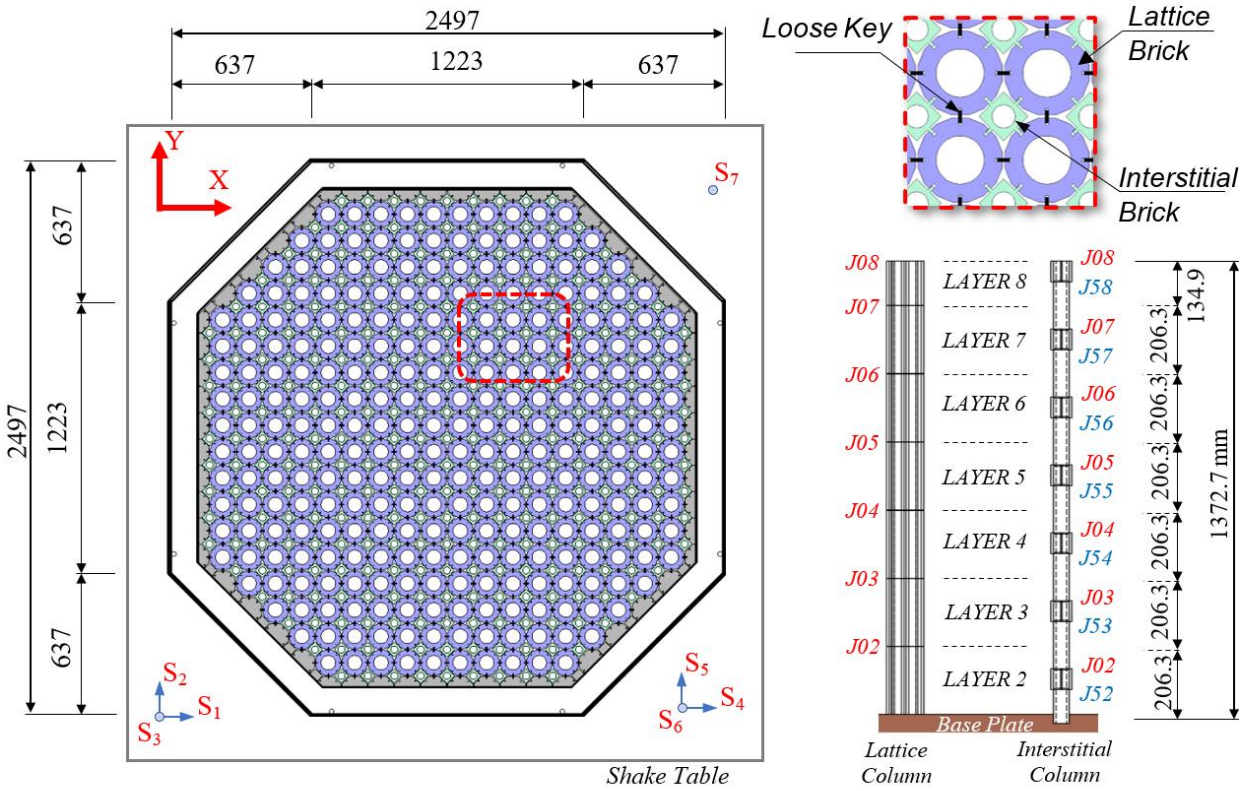

Fig. 2. Plan view of the MLA along with X and Y position coordinates, with detail of the lattice and interstitial columns – all dimensions in mm.

Fig. 3. Detail of each brick type used within the Multi-Layered Array: (a) instrumented interstitial brick; (b) instrumented filler brick; (c) lattice brick; (d) instrumented lattice brick; (e) doubly-cracked lattice brick; (f) instrumented doubly-cracked lattice brick; (g) triply cracked lattice brick; (h) quadruply cracked lattice brick

In this study, the multi-layered array configurations; MLA01, MLA10, MLA11 and MLA13 are presented providing a comparison between an intact and multiply cracked configurations for the same input seismic motion, 0.4g HPB motion in the shaking table x-direction. See Figure 1 for the global shaking table coordinate system. MLA01 is the intact array providing reference results of an uncracked array. The MLA10 configuration comprises of 143 Multiply Cracked Bricks (MCBs), both symmetric and asymmetric triply cracked, and 427 Doubly Cracked Bricks (DCBs) total cracked bricks distributed over layers 4-7. MLA11 was configured to contain 229 MCBs and 341 Doubly Cracked Bricks total cracked bricks integrated within layers 4-7. MLA13's cracked brick configuration was similar to MLA11 still containing approximately 50% cracked bricks within layers 4-7, however, disconnected at the array boundary. The location of the cracked bricks differs between each MLA. The variation in crack arrangement and distribution between different MLA configurations modelled the state of an AGR core at different points in its lifespan, with the intent to evaluate the influence of degraded and irradiated bricks, and the significance of cracking, on the global mechanical behaviour of the MLA. Interstitial brick column IB2226, for the MLA10 configuration, is presented as a case-study for demonstration of the mathematical procedure in converting calibrated interface measurements into the global column shape displacement profiles.

3. Calculation of Column Shape Displacements

Each MLA experiment has a unique configuration of instrumented columns and IDCBs. A single experiment comprises up to 100 individual tests which are representative of a range of seismic events. The displacement measurements acquired at the column interfaces enables the column shape profile to be calculated for each test. To process the raw data to column shape profiles, the sensor data from each interface must be calibrated and then converted from the local coordinate system to the global coordinate system. The challenge associated with identifying the column displacement relates to the fact that the displacement data recorded at each instrumented interface is relative, not absolute. As a result, it is not possible to directly calculate the displacement along the entire column.

As detailed in Section 2, the components that comprise the bottom layer of the array are restrained, and their positions are geometrically fixed to the base plate. Using the known position of the bottom brick in the column enables the position of the second layer brick to be inferred based on the relative displacement recorded at the brick interface. In this manner, the column shape profile can be estimated by cumulatively summing the position, and rotational contributions, of each individual brick interface within the column. This is computed iteratively utilising an Euler mechanics procedure. Once the column shape profile has been calculated using the interface data, the computed displacement of the top brick in the column is compared against the trajectory as recorded by the motion capture vision system.

3.1. Interstitial columns

Calibration of the Hall Effect sensor data is non-trivial as it needs to account for the inherent non-linearity of the sensors and the fact that the interface motion is fully coupled in all six degrees of freedom. To obtain meaningful results from the raw data, a reference data set was used to generate a linearly independent eighth-order polynomial fit using a nonlinear system identification technique. The resulting 'calibration volume' could then be applied to the raw data to convert the sensor measurements to six degree of freedom motion data. The following discussion describes the data processing techniques after

the raw sensor data has been converted to meaningful measurements in SI units. Please refer to Oddbjornsson et al. (2021) for a complete discussion of the calibration method.

The acquired displacement data consists of horizontal translations in x and y, vertical translation in z, with corresponding rotations: roll (φ), pitch (θ) and yaw (ψ) about the x, y, z axes respectively. The displacements are a measurement of the relative movement at the interface between two bricks, and as such are recorded in a local frame of reference. To calculate the column displacement, the interface data must first be transformed to the global shaking table coordinate system and then projected to the centre of gravity (CoG) for each interstitial and filler brick. These two operations can be combined to yield a single transformation matrix which accounts for the orientation of each brick column with respect to the global coordinate system and converts the interface displacement to displacement at the brick CoG. Prior knowledge of physical brick geometry is required to evaluate a brick's CoG successfully.

Interstitial columns are typically oriented at ±90º to the MLA global axes, for ease of installation and building of a specific MLA configuration. It was considered problematic to try build an MLA with zero relative rotation to the global shaking table coordinate system. This results in the following transformation matrices to account for the column orientation:

$$R0 = R_{\psi}(90) = \begin{bmatrix} 0 & -1 & 0 & 0 \\ 1 & 0 & 0 & 0 \\ 0 & 0 & 1 & 0 \\ 0 & 0 & 0 & 1 \end{bmatrix}, \qquad RF0 = R_{\psi}(-90) = \begin{bmatrix} 0 & 1 & 0 & 0 \\ -1 & 0 & 0 & 0 \\ 0 & 0 & 1 & 0 \\ 0 & 0 & 0 & 1 \end{bmatrix} \tag{1}$$

where *R0* is the matrix applied to columns with a +90º rotation, and RF0 is the matrix for columns rotated at -90º with respect to the MLA global coordinate system and R_{ψ} is the Euler rotation transformation matrix applied about the vertical, *z*, axis. This is defined in equation 4.

To project the interface data to the brick CoG, the matrices *R0* and *RF0* are multiplied by the geometric transformation matrices which are specific to the brick type, filler or interstitial. Taking a column orientation of -90º as an example, the motion at the CoG of a filler brick in global coordinates can be calculated by applying the following matrix, *GCFB*, to the interface data:

$$GCFB = RF0 \times GCFB = \begin{bmatrix} 0 & 1 & 0 & 0 \\ -1 & 0 & 0 & 0 \\ 0 & 0 & 1 & 0 \\ 0 & 0 & 0 & 1 \end{bmatrix} \times \begin{bmatrix} 0 & 0 \\ 0 & 0 \\ (\frac{Ih}{2} - Fh) & (Ih/2) \\ 1 & 1 \end{bmatrix} = \begin{bmatrix} 0 & 0 \\ 0 & 0 \\ (\frac{Ih}{2} - Fh) & (Ih/2) \\ 1 & 1 \end{bmatrix} \tag{2}$$

where *Ih* is the height of an interstitial brick and *Fh* is the height of the filler brick.

The equivalent matrix for an interstitial brick, denoted *GCIB*, is defined as follows:

$$GCIB = RF0 \times GCIB = \begin{bmatrix} 0 & 1 & 0 & 0 \\ -1 & 0 & 0 & 0 \\ 0 & 0 & 1 & 0 \\ 0 & 0 & 0 & 1 \end{bmatrix} \times \begin{bmatrix} 0 & 0 & 0 & 0 \\ 0 & 0 & 20.025 & 20.025 \\ \left(-\frac{Ih}{2}\right) & \left(\frac{Ih}{2}\right) & \left(-\frac{Ih}{2}\right) & \left(\frac{Ih}{2}\right) \\ 1 & 1 & 1 & 1 \end{bmatrix}$$

$$= \begin{bmatrix} 0 & 0 & 20.025 & 20.025 \\ 0 & 0 & 0 & 0 \\ \left(-\frac{Ih}{2}\right) & \left(\frac{Ih}{2}\right) & \left(-\frac{Ih}{2}\right) & \left(\frac{Ih}{2}\right) \\ 1 & 1 & 1 & 1 \end{bmatrix} \tag{3}$$

Note, the quantity 20.025mm refers to the interstitial brick's bore radius, the distance of the interstitial brick from the inner circular perimeter to its geometric centre. See Figure 3(a&b) for a visual understanding.

To calculate the position of each brick in a column based on the position of the bottom layer brick, Euler rotation matrices are applied to the interface measurements in all 6 DoF. The rotation matrices are defined as follows:

$$Rx\,(R_\varphi) = \begin{bmatrix} 1 & 0 & 0 & 0 \\ 0 & \cos(\varphi) & -\sin(\varphi) & 0 \\ 0 & \sin(\varphi) & \cos(\varphi) & 0 \\ 0 & 0 & 0 & 1 \end{bmatrix}, \tag{4a}$$

$$Ry\,(R_\vartheta) = \begin{bmatrix} \cos(\theta) & 0 & \sin(\theta) & 0 \\ 0 & 1 & 0 & 0 \\ -\sin(\theta) & 0 & \cos(\theta) & 0 \\ 0 & 0 & 0 & 1 \end{bmatrix}, \tag{4b}$$

$$Rz\,(R_\psi) = \begin{bmatrix} \cos(\psi) & -\sin(\psi) & 0 & 0 \\ \sin(\psi) & \cos(\psi) & 0 & 0 \\ 0 & 0 & 1 & 0 \\ 0 & 0 & 0 & 1 \end{bmatrix} \tag{4c}$$

where R_φ/R_x is the rotation about the x-axis, R_ϑ/R_y is the rotation about the y-axis and R_ψ/R_z is the rotation about the z-axis.

The translation transformation matrix describing the translational motion associated with the rotations acquired at a particular interface is defined as follows:

$$T = \begin{bmatrix} 1 & 0 & 0 & x \\ 0 & 1 & 0 & y \\ 0 & 0 & 1 & z \\ 0 & 0 & 0 & 1 \end{bmatrix} \tag{5}$$

For an interstitial brick column, a single brick layer is characterised by both top and bottom brick interface measurements. These are denoted as *J0x* and *J5x* for bottom (filler) and top (interstitial) brick interface measurements respectively (see Figure 2). The calculation of the position of each brick in the column is determined for each interface using the following set of equations:

$$TC\_02 = RF0 \times R0 \times T\_J52 \times Rz\_J52 \times Ry\_J52 \times Rx\_J52 \times GCFB \quad (6a)$$

$$TC\_53 = TC\_02 \times T\_J02 \times Rz\_J02 \times Ry\_J02 \times Rx\_J02 \times GCIB \quad (6b)$$

$$TC\_03 = TC\_53 \times T\_J53 \times Rz\_J53 \times Ry\_J53 \times Rx\_J53 \times GCFB \quad (6c)$$

$$TC\_54 = TC\_03 \times T\_J03 \times Rz\_J03 \times Ry\_J03 \times Rx\_J03 \times GCIB \quad (6d)$$

$$TC\_04 = TC\_54 \times T\_J54 \times Rz\_J54 \times Ry\_J54 \times Rx\_J54 \times GCFB \quad (6e)$$

$$TC\_55 = TC\_04 \times T\_J04 \times Rz\_J04 \times Ry\_J04 \times Rx\_J04 \times GCIB \quad (6f)$$

$$TC\_05 = TC\_55 \times T\_J55 \times Rz\_J55 \times Ry\_J55 \times Rx\_J55 \times GCFB \quad (6g)$$

$$TC\_56 = TC\_05 \times T\_J05 \times Rz\_J05 \times Ry\_J05 \times Rx\_J05 \times GCIB \quad (6h)$$

$$TC\_06 = TC\_56 \times T\_J56 \times Rz\_J56 \times Ry\_J56 \times Rx\_J56 \times GCFB \quad (6i)$$

$$TC\_57 = TC\_06 \times T\_J06 \times Rz\_J06 \times Ry\_J06 \times Rx\_J06 \times GCIB \quad (6j)$$

$$TC\_07 = TC\_57 \times T\_J57 \times Rz\_J57 \times Ry\_J57 \times Rx\_J57 \times GCFB \quad (6k)$$

$$TC\_58 = TC\_07 \times T\_J07 \times Rz\_J07 \times Ry\_J07 \times Rx\_J07 \times GCIB \quad (6L)$$

$$TC\_08 = TC\_58 \times T\_J58 \times Rz\_J58 \times Ry\_J58 \times Rx\_J58 \times GCFB \quad (6m)$$

Where *TC* is the locally stored vector-matrix algebraic result for interface *5x* or *0x* for each layer respectively.

The column shape estimate is then calculated by cumulatively summing the position of each individual brick at each time step to build the fully processed time-history datasets. Filler and interstitial bricks are differentiated between each other by applying the geometric nodal plane transformation matrices, GCIB & GCFB, as defined in equation 2 and 3.

Figure 4 shows a typical calibrated time-history for a single layer of interstitial brick column IB2226 for the MLA10 configuration with an input 0.4g HPB motion in the x-direction. Filler brick interface measurements are illustrated in blue whilst an interstitial is displayed in black for layer 3, interface J03 and J53 respectively. Figure 4(a)-(c) illustrate the translations whilst (d)-(f) display the rotations about the local brick interface x, y, z axes respectively. The waveforms of each brick type display similar motion illustrating the interfaces as being either in- or out-of-phase. This is evident in Figure 4(b&d).

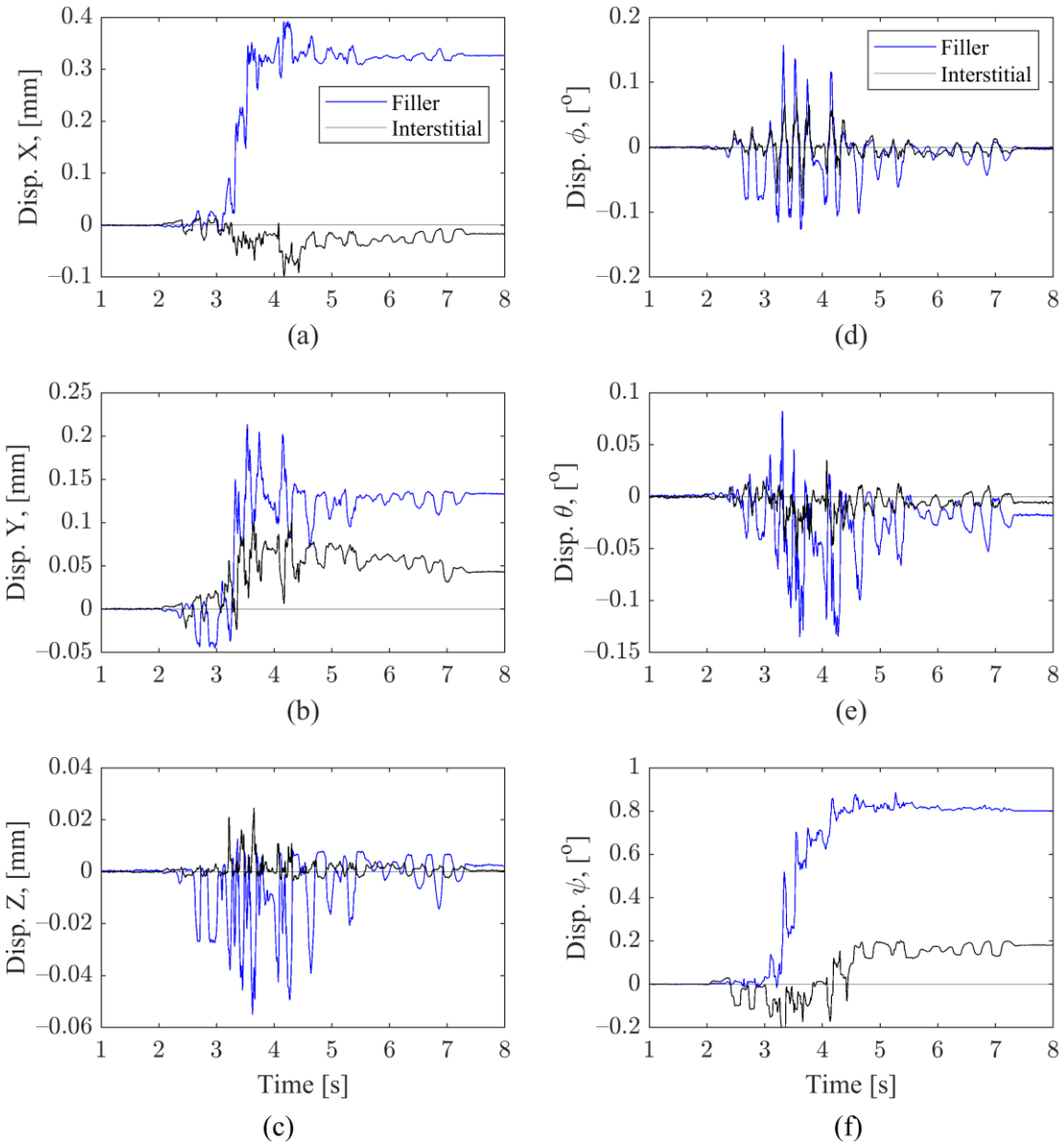

Fig. 4. Displacement time history of calibrated interstitial column IB2226 for MLA10 with an input seismic 0.4g HPB motion in the x direction for filler and interstitial brick interfaces (a) horizontal translation X; (b) horizontal translation Y; (c) vertical translation Z; (d) rotation about x axis, φ; (e) rotation about y axis, θ; (f) rotation about z axis, ψ.

3.2. Lattice columns

To convert the single-axis vertical displacement data, *z*, recorded by the LCPs to column shape profiles, basic trigonometry was applied to calculate the values of roll, φ, and pitch, θ, at each brick interface. A minimum of three LCPs were required for the calculation of all variables, hence the installation of four sensors per interface provided redundancy in the case of sensor failure. When data is available from all four sensors, each LCP pair is used to calculate a local value for roll and pitch. The mean value for roll and pitch is then calculated from the individual results of each LCP pair. Presented in Figure 5 is a schematic of the LCP layout and the method by which values for roll, φ, and pitch, θ, can be derived based on the vertical z displacement and known geometry of individual sensors.

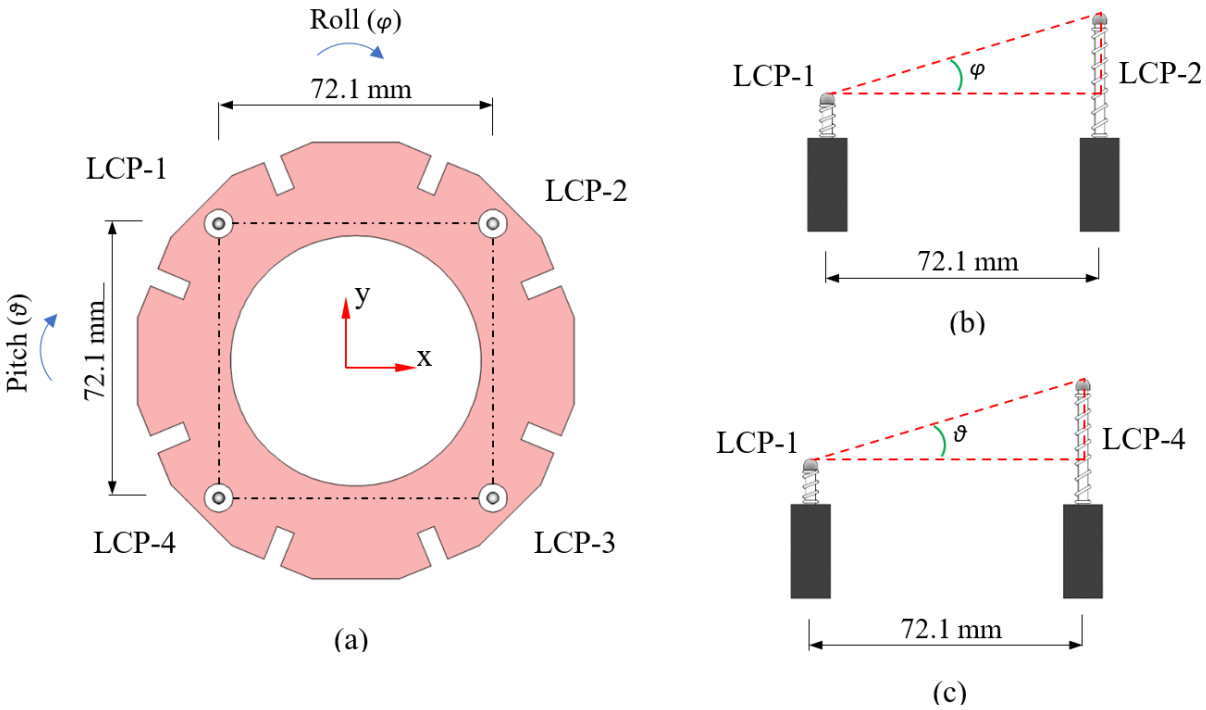

Fig. 5. Procedure to evaluate roll and pitch rotations using vertical sensor displacement measurements, (a) schematic plan view of top/bottom of instrumented lattice brick; (b) trigonometric side-elevation evaluation of roll, φ, angle measurement using LCP_1 and LCP_2; (c) trigonometric side-elevation evaluation of pitch, θ, angle measurement using LCP_1 and LCP_4

Following the procedure demonstrated in Figure 5, the local relative lattice interface roll and pitch estimates are evaluated using the following equation,

$$\varphi_{LCS} = \tan^{-1}\left(\frac{Z_{LCP2} - Z_{LCP1}}{72.1}\right), \qquad \vartheta_{LCS} = \tan^{-1}\left(\frac{Z_{LCP4} - Z_{LCP1}}{72.1}\right) \tag{7}$$

where φ_{LCS} and ϑ_{LCS} are the local roll and pitch evaluated, and $Z_{LCP1} - Z_{LCP4}$ are the individual local vertical displacements describing each LCP for a single interface. The value of 72.1mm denotes the distance between the centre of two LCP sensors.

Similar to interstitial columns, lattice columns are typically oriented at three different angles, ±157.5º and 112.5 with respect to the MLA global shaking table coordinate axes. To account for the column orientation, the global rotations about a specific lattice brick interface are identified as follows,

$$\varphi = \varphi_{LCS}\cos(\pm 157.5) - \vartheta_{LCS}\sin(\pm 157.5) \tag{8a}$$

$$\vartheta = \varphi_{LCS}\sin(\pm 157.5) + \vartheta_{LCS}\cos(\pm 157.5) \tag{8b}$$

where φ and ϑ are the global roll and pitch displacement rotations evaluated. The vertical displacement trajectory, Z, is evaluated as the mean of the four individual vertical displacement measurements.

Figure 6 displays a typical calibrated and processed interface time-history for lattice brick column LB2325 for the MLA10 configuration with an input 0.4g HPB motion in the x-direction. Figure 6(a)

illustrates the vertical translation whilst (b) and (c) display the rotations about the local brick interface x, and y axes respectively.

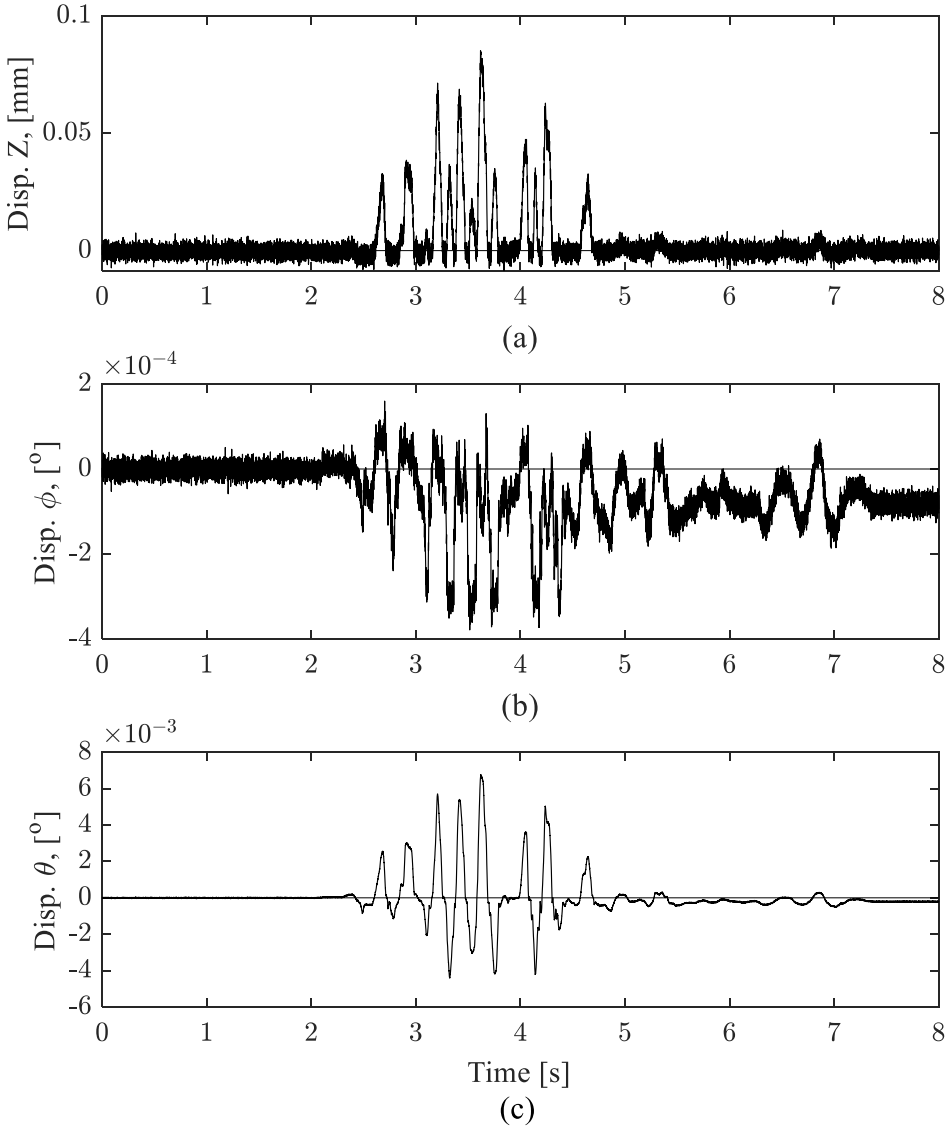

Fig. 6. Displacement time history of calibrated lattice column LB2325 measurements for MLA10 with an input seismic 0.4g HPB motion in the x direction for a lattice brick interface (a) vertical translation Z; (b) rotation about x axis, φ; (c) rotation about y axis, θ

Similarly to the interstitial column interface measurements, the Euler rotation matrices, defined in equation 4, are required to identify the position of each brick in a lattice column based on the position of the bottom layer brick. As only roll and pitch estimates are available, equation 4(b&c) are applied and constructed per time-step of a time-series with vertical translations stored using the translation matrix defined in equation 5. A lattice column is characterised by seven measured bottom interfaces, J02-J08 given in Figure 2, and therefore to evaluate the column shape, equations 6(a, c, e, g, i, k & m) are applied. i.e. applying the odd interface computations. These are calculated cumulatively summing the position of each individual brick at each time step to build the complete time-histories. The conversion from the local interface to global shaking table coordinate system has already been identified in evaluated the global roll and pitch measurements. Therefore, the rotation matrices *R0* and *RF0* are not required in computing the column shapes as needed for the interstitial brick column type.

To project the processed column shape data, *TC*, per interface to the brick CoG, the geometric transformation matrices specific to the lattice brick types, representing a full size brick, GCLB, and the two-thirds sized top brick, GCTLB, are applied (instead of GCIB and GCFB used in the interstitial and filler computations). These are shown as,

$$GCLB = \begin{bmatrix} 0 & 0 & & 0 & 0 & 0 \\ 0 & 0 & 0 & 48.125 & & 48.125 \\ 0 & \left(\frac{Lh}{2}\right) & & Lh & 0 & Lh \\ 1 & 1 & & 1 & 1 & 1 \end{bmatrix} \tag{9a}$$

$$GCTLB = \begin{bmatrix} 0 & 0 & & 0 & 0 & 0 \\ 0 & 0 & 0 & 48.125 & & 48.125 \\ 0 & (TLh/2) & & TLh & 0 & TLh \\ 1 & 1 & & 1 & 1 & 1 \end{bmatrix} \tag{9b}$$

where *Lh* is the height of a full sized lattice brick and *TLh* is the height of the two-thirds sized lattice bricks located on the top layer, J08. The 48.125mm refers to the lattice brick bore radius, the distance from the inner circular perimeter to the geometric centre.

Figure 7 shows the time-history of the evaluated column shape displacements for lattice brick column LB2325 for the MLA10 build configuration subject to an input 0.4g HPB motion in the x-direction. Stacked brick column x-displacement trajectories are displayed for J02-J08. Interestingly, the largest displacement amplitudes are exhibited at interface J06 and J07 with reduced motion at J08. For this specific test, column LB2325 measurements indicate that the largest responses do not occur at the top of the stacked column. This is common through all tests and test configurations and is likely due to the intact top layer. J02 exhibits very small amplitudes indicative of the rigid base boundary effect.

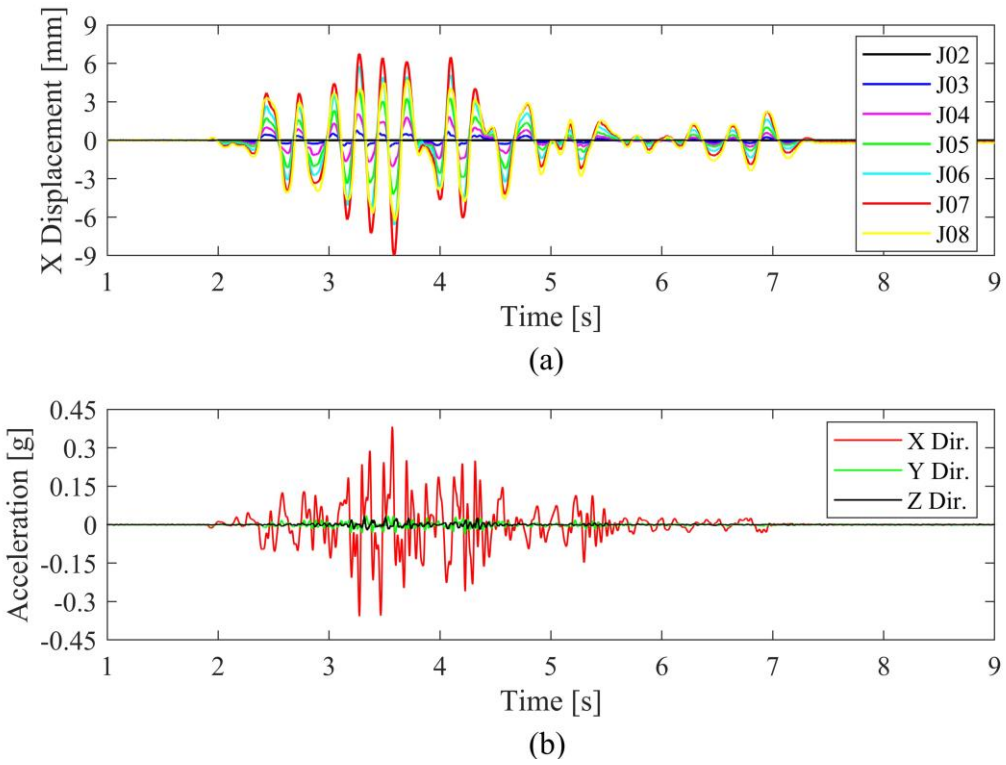

Fig. 7. Time history responses for MLA10 with an input seismic 0.4g HPB motion in the x-direction (a) Global displacement time history of computed column shape data for lattice column LB2325; (b) Recorded shaking table acceleration time history in x, y and z directions

3.3. IR motion capture

The displacement of the top brick in each instrumented column, as measured by the vision system, was used to verify the computed column shape displacements using the LCP and Hall effect interface sensor measurements. Each of the three IR markers attached to each individual brick column top layer yielded a displacement dataset. To reduce the vision system results to a single displacement measurement per brick, the mean value of the three markers was calculated. This mean trajectory was then converted from the vision system's absolute frame of reference to the brick relative frame of reference to enable direct comparison with the displacement data calculated from the column interface measurements. These are presented as a comparison in Section 5 to evaluate the performance of the indirect column shape algorithm.

4. Computed Lattice and Interstitial Column Shape Profiles

There have been a large number of experiments conducted using the MLA as part of a test programme that has spanned many years. Thirteen different array configurations have been shaken more than 3000 times to characterize the dynamic response of the AGR core model under seismic excitation with emphasis on array distortion and the shape of the column profiles. The MLA01 configuration is an intact array which is composed of eight layers representing the inner ten octagonal rings of an AGR core. For the MLA10 configuration, 50% of the bricks comprising layers four through seven consisted of either doubly or triply cracked bricks. The MLA11 configuration also included quadruply cracked bricks in addition to doubly and triply cracked bricks. For MLA11 the cracked bricks made up 50% of

the bricks installed in layers four to seven. For MLA13, the shear keying system was removed between the fixed boundary and the outer most ring of active bricks within layers two to seven of the array.

Column shape distortion profiles are presented for interstitial columns IB2622 and IB2226 in Figure 8 with lattice columns LB2325 and LB3319 displayed in Figure 9, respectively. For each instrumented brick column, displacement profiles are evaluated for configurations MLA01 (in blue), MLA10 (in black), MLA11 (in red) and MLA13 (in green) under seismic HPB10^{-4} input motion in the x-direction with a peak forcing amplitude of 0.4g. This demonstrates the influence of the different crack configurations and distributions within an MLA on the global column behaviour when subject to input seismic excitation. Distortion profiles are evaluated using the computed column shape time-history responses and identifying the maxima and minima within each record per brick interface. These are identified for both horizontal x- and y- directions and plotted as a function of the global vertical 'z' measurements. Analysing the data in this manner enables visualisation of the maximum displacement envelope exhibited by an instrumented brick column during dynamic/seismic loading.

Figures 8(a&c) and 9(a&c) demonstrate similar behaviour for the computed column shape distortion profiles of interstitial and lattice columns in the x-direction, corresponding to the direction of the input seismic excitation. The displacement envelope is observed to increase linearly with the largest amplitudes exhibited at around layer six reducing in significant magnitude at layer eight. Interestingly, the response of MLA01 for each instrumented column, which corresponds to an intact array, increases linearly with column height following a distinctly different distortion profile to MLA10, MLA11 and MLA13, which correspond to cracked configurations. This would suggest that for an intact array, columns behave in a conceptually similar manner to an inverted pendulum demonstrating swaying motion when subjected to dynamic/seismic loading. The column profiles for the cracked configurations are observed to follow similar envelopes, both in trends and amplitudes, suggesting that the behaviour of both interstitial and lattice columns are dependent on the presence of cracked bricks with a level of insensitivity to cracking configuration and/or distributions at the high 50% proportion of cracking investigated. However, the x-direction column shape for IB2226 indicates a double maximum between layers 5-7 with similar amplitudes. It does follow similar profiles to IB2622 in Figure 8(c). Distortion profiles in the y-direction exhibit considerably low displacement amplitudes for each column indicating that the response of a column is dominated by the direction of the input dynamic loading. Lattice column LB3319, as shown in Figure 9(d), does however display similar responses envelopes for both x- and y-directions. The amplitudes at layer six are considerably less for the y-direction. Displacements are particularly apparent for the MLA13 build configuration. For the other columns presented, this y-direction behaviour is not observed.

Residual displacement analysis is performed to identify whether a brick column is capable of returning to its initial static conditions after being dynamically excited. That is, identifying if the displacement at time zero of the test is approximately equal to the displacement at the end of testing. On average, for both instrumented lattice and interstitial columns, residual displacements were identified to be 0.02mm and 0.03mm, for x- and y-directions, with a standard deviation of 0.02mm and 0.04mm respectively. These indicate low coefficients of variation demonstrating uniform low dispersion of the residual displacement amplitudes for each column type. Therefore, it is a reasonable assumption to state brick columns return to their static initial conditions after dynamic loading. This phenomena can be described by the radial and axial keying system implemented within the build of an MLA configuration (Dihoru et al., 2017).

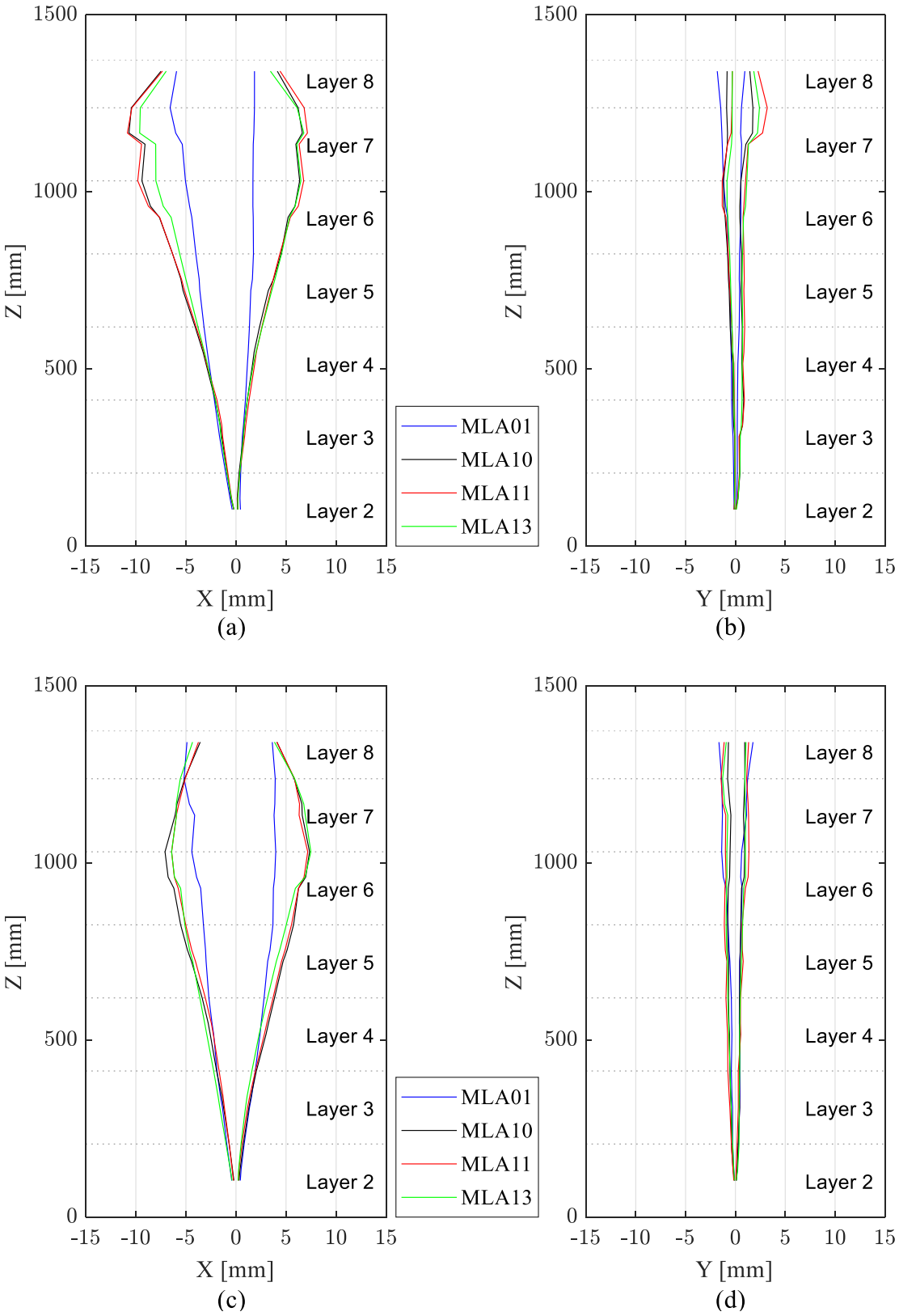

Fig. 8. Interstitial brick column displacement/distortion profiles for input x-direction HPB seismic motion with a forcing amplitude of 0.4g for MLA1, MLA10, MLA11 and MLA13 build configurations, (a) IB2226 x direction; (b) IB2226 y direction; (c) IB2622 x direction; (d) IB2622 y direction

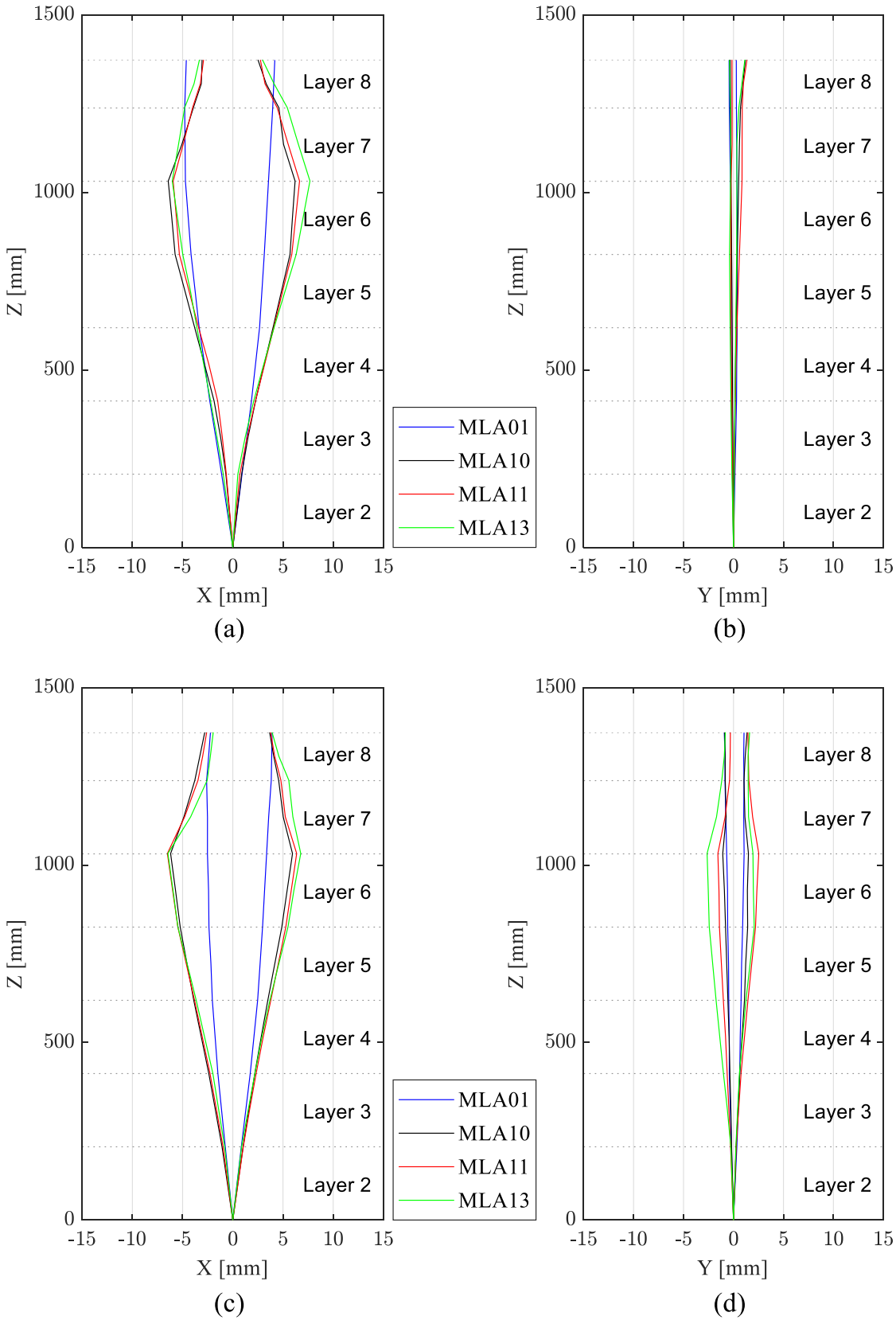

Fig. 9. Lattice brick column displacement/distortion profiles for input x-direction HPB seismic motion with a forcing amplitude of 0.4g for MLA1, MLA10, MLA11 and MLA13 build configurations, (a) LB2521 x direction; (b) LB2521 y direction; (c) LB3319 x direction; (d) LB3319 y direction

5. Assessment of Computed Column Shapes

5.1. Column shape algorithm performance

To verify the column shape distortion profiles for each instrumented column, as calculated from the μDAQ measurements, results were compared against the top brick displacement measurements captured by the vision system. Presented in Figures 10 and 11 are comparative plots of the calculated and measured displacements of the top brick of an interstitial column, IB2622, with results for an instrumented lattice brick column, LB2521, shown in Figures 12 and 13. The displacement calculated from the μDAQ data is shown in blue, with the corresponding results from the vision system measurements presented in black. The results are taken from a test in the MLA10 configuration at a 0.4g target amplitude, with a HPB seismic input motion in the x-direction. Refer to Figure 2 for the shaking table global coordinate system.

Figures 10 and 11 present the top brick displacement time histories for an interstitial column along with the absolute difference between the μDAQ and vision results in the x- and y-direction, respectively. As shown in Figure 10, there is good agreement between results in phase, frequency, and amplitude in the x-direction. At time instances 3.5s and 4.5s there is a 1mm discrepancy in the amplitude between the μDAQ and vision system results, and smaller deviations of approximately 0.2mm can also be seen at other local maxima and minima. Despite these discrepancies the comparison between the two data sets is favourable. In the y-direction, as presented in Figure 11, the μDAQ and vision system data initially yield similar results, however at approximately 4s there is a clear deviation. The subsequent discrepancy between the data sets increases to 0.9mm, which represents 70% of the peak displacement magnitude. There is also a shift in the overall mean amplitude of the μDAQ result suggesting there may be a sensor drift associated with the column profile instrumentation. Even though the μDAQ result becomes offset in time when compared to the vision system data, the two y-direction results yield a favourable comparison in phase and frequency. In addition, although there is an obvious discrepancy in the absolute values of amplitude in the y-direction, the trend is consistent between the two data sources.

Figures 12 and 13 present the top brick displacement time histories for a lattice column along with the absolute difference between the μDAQ and vision results in the x- and y-direction, respectively. In the x-direction similar results are obtained from both the μDAQ and vision system data, with very good alignment in phase, frequency, and amplitude. In the y-direction there is the same amplitude drift over time as seen in the interstitial column results. Despite the discrepancy in the absolute value of amplitude in the y-direction, the trend shown by the μDAQ result remains consistent with the vision system data. The y-direction results compare favourably in phase and frequency between the μDAQ and the vision system data. In general, the observed deviations in the x- and y-directions for both lattice and interstitial columns are of similar magnitude. It should be noted that the differences exhibited in the y-direction time-histories may be amplified by the smaller magnitude of motion, relative to the x-direction, observed during dynamic testing.

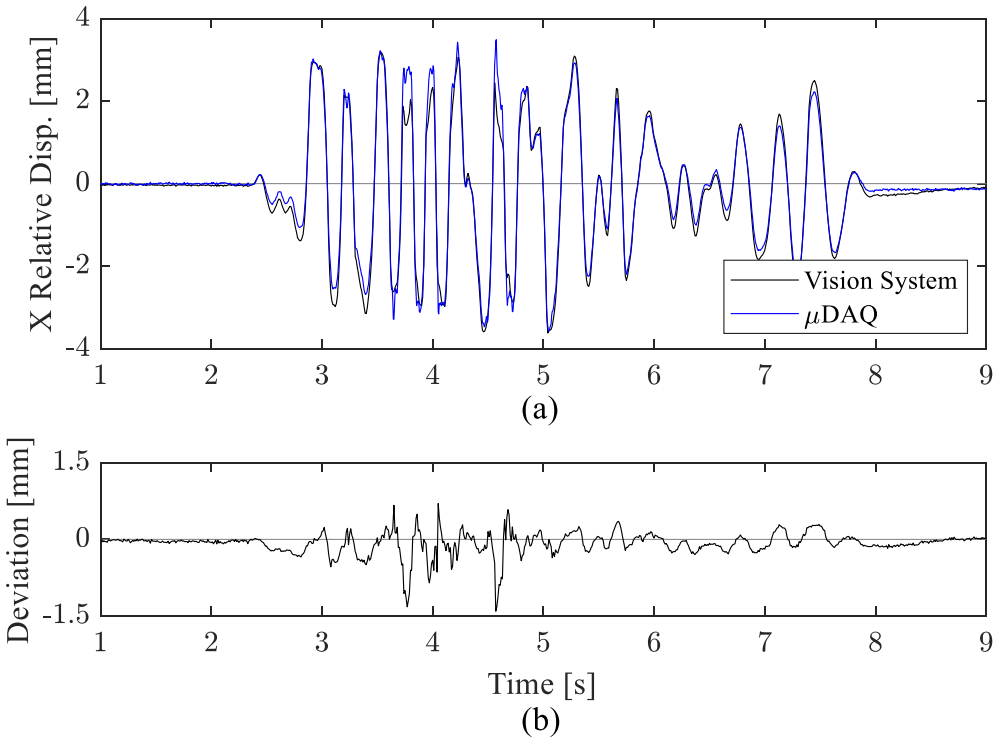

Fig. 10. Comparison of top brick relative displacement using computed column shape data (in blue), for interstitial column IB2622, and a separate displacement tracking vision system (in black) for MLA10 with an input seismic 0.4g HPB motion in the x direction, (a) relative displacement time-histories; (b) deviation time-history (vision system to μDAQ)

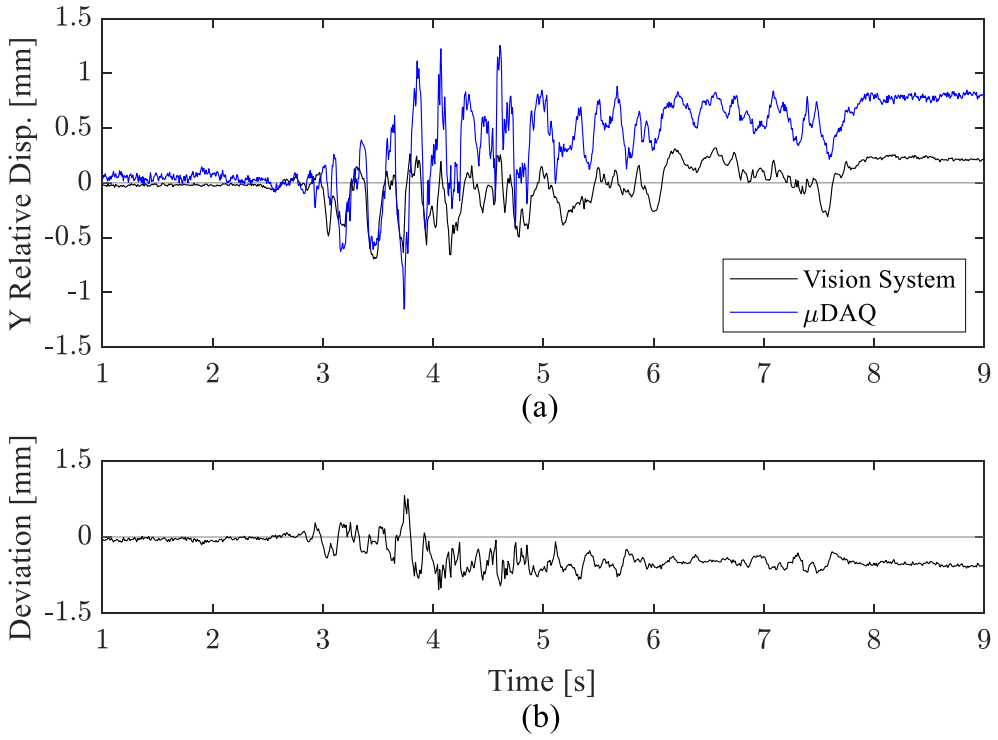

Fig. 11. Comparison of top brick relative displacement using computed column shape data (in blue), for interstitial column IB2226, and a separate displacement tracking vision system (in black) for MLA10 with an input seismic 0.4g HPB motion in the y direction, (a) relative displacement time-histories; (b) deviation time-history (vision system to μDAQ)

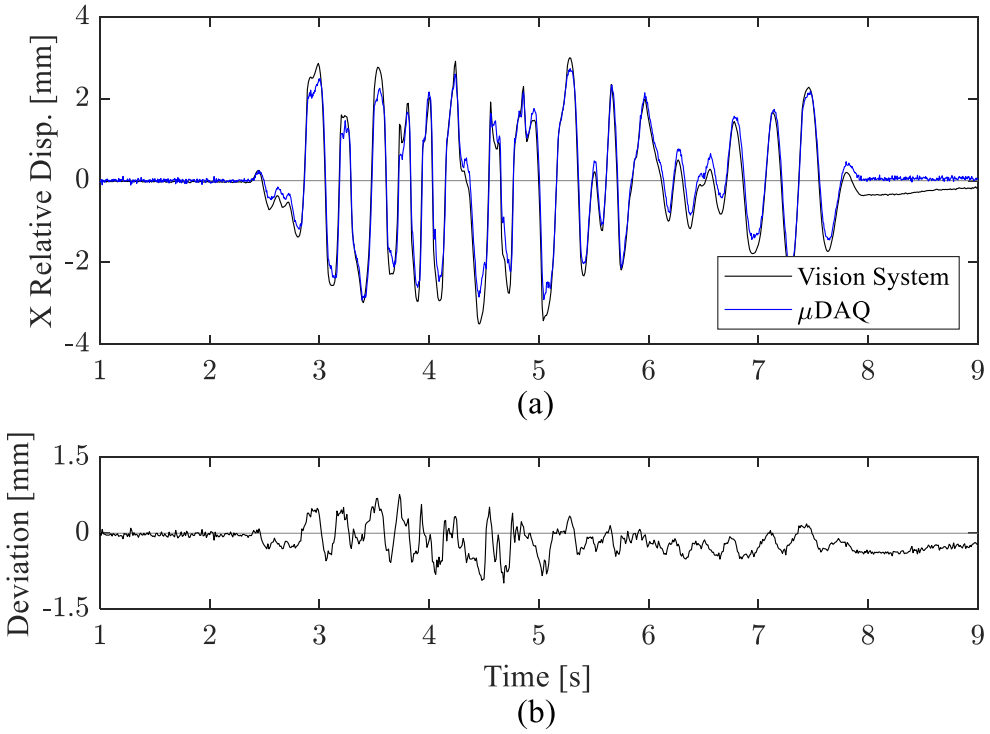

Fig. 12. Comparison of top brick relative displacement using computed column shape data (in blue), for lattice column LB2521, and a separate displacement tracking vision system (in black) for MLA10 with an input seismic 0.4g HPB motion in the x direction, (a) relative displacement time-histories; (b) deviation time-history (vision system to μDAQ)

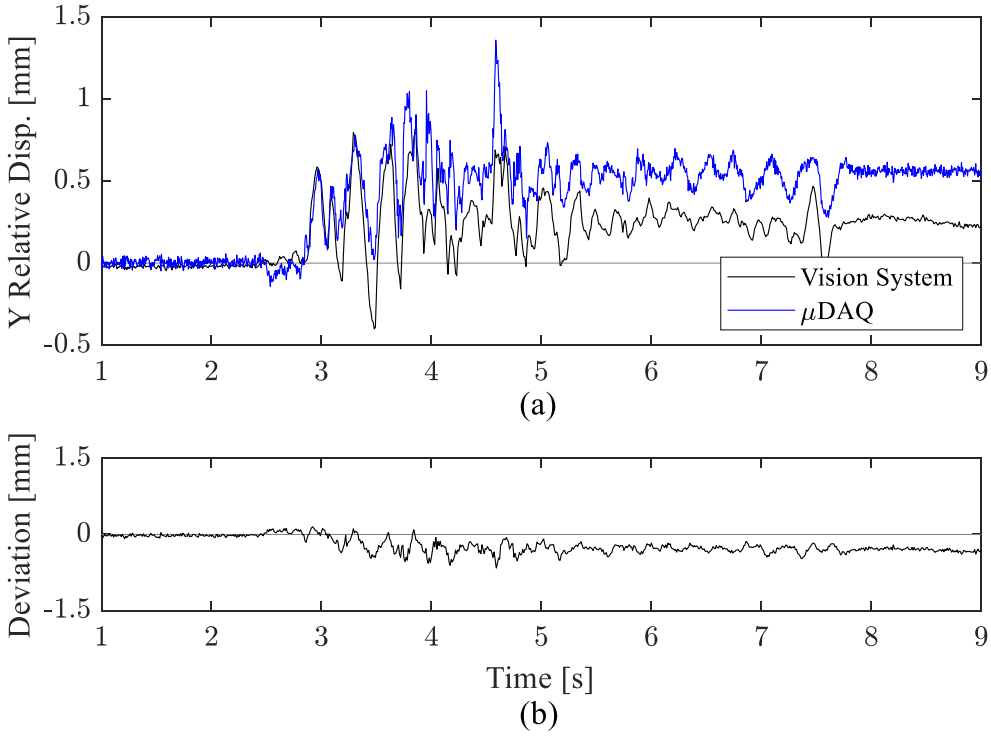

Fig. 13. Comparison of top brick relative displacement using computed column shape data (in blue), for lattice column LB2521, and a separate displacement tracking vision system (in black) for MLA10 with an input seismic 0.4g HPB motion in the y direction, (a) relative displacement time-histories; (b) deviation time-history (vision system to μDAQ)

5.2. Statistical analysis

A statistical analysis of the two top brick column shape displacement waveforms is performed to quantify the performance of the uDAQ measurements, for all MLA configurations discussed and explored in Section 4. As the vision system displacement signal is the only comparison signal, our own metrics are constructed and presented to quantitatively summarise the performance of the indirect column shape displacement evaluation algorithm. This does assume that the displacement signals acquired by the motion capture vision system are precise and accurate, an assumption belied by the manufacturer's claim of ± 0.05mm tracking accuracy and a potential for other sources of uncertainty resulting from the testing setup. Examples such as camera mount vibration, marker mount imperfection and visual noise. Direct analysis of the two signals is carried out evaluating the Pearson correlation followed by evaluating the differentiation/deviation in time between the two measurement sources. The mean, standard deviation and coefficient of variation, representing the relative standard deviation, of the deviation time-histories are computed over the active response time-window of the input seismic motion corresponding to the time interval 2-8s, as shown in Figures 10(b)-13(b). Analyses are performed for both x and y time-history signals.

Figure 14 visualises the qualitative correlation between the uDAQ and motion capture vision system dataset, previously presented in Figure 10-13. Figure 14(a&b) represent the interstitial and lattice brick columns, IB2622 and LB2521 respectively for both x (in black) and y (in blue) axis directions respectively. For the x-displacement data, both brick columns correlate well giving good agreement in the observations acquired. The y-displacement matches well for the lattice brick column while drift and a poorer correlation is exhibited for the interstitial column. This qualitative analysis is used to guide the statistical quantitative analysis in assessing the performance of the indirect column shape displacement algorithm developed herein.

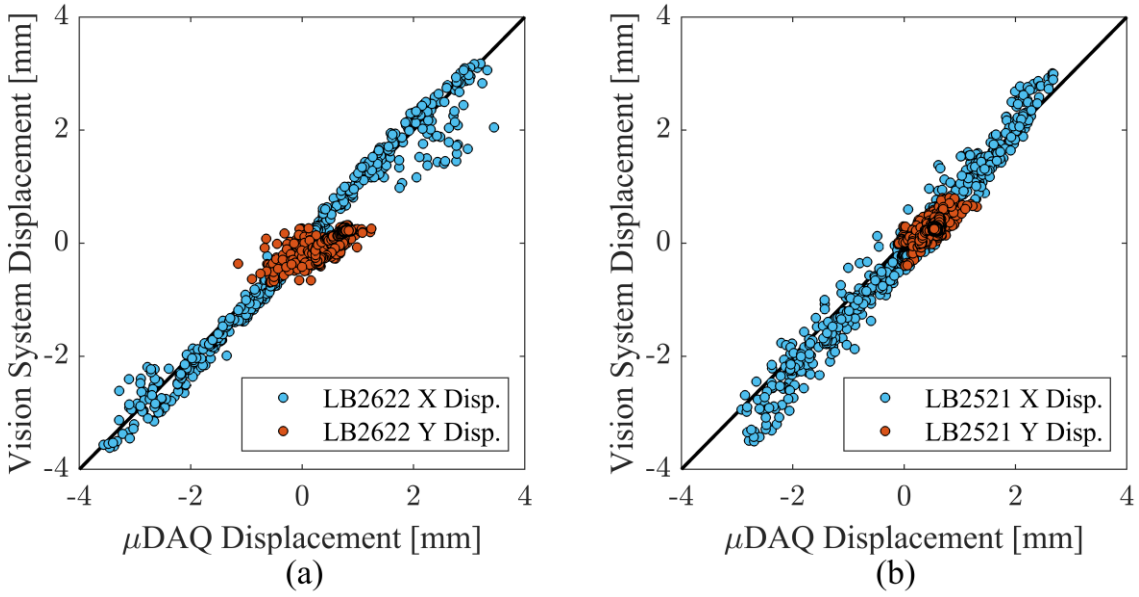

Fig. 14. Correlation of top brick relative displacement between computed column shapes from μDAQ measurements and a separate displacement tracking vision system for MLA11 with an input seismic 0.4g HPB motion in the x direction, (a) Interstitial brick column IB2622 correlation ; (b) Lattice brick column LB2521 correlation

Table 1 provides a statistical assessment of the performance of the indirect column shape displacement evaluation at the centre of the top of a brick column as compared to a separate motion capture vision displacement tracking system. The Pearson correlation between the two trajectories, mean, standard deviation and coefficient of variation of the deviation time-history, comparing the vision system data to the µDAQ system data, are computed. The deviation time-history is evaluated as the difference between the two systems with respect to the vision system. These are identified for both the global x- and y-directions for instrumented interstitial and lattice brick columns, IB2226, IB2622, LB2521 & LB3319, for MLA01, MLA10, MLA11 and MLA13 build configurations subject to HPB seismic input excitation in the x-direction at a target amplitude of 0.4g. Figures 10-13 demonstrate typical specific instrumented brick column time-histories. Initial qualitative assessment suggests good agreement of indirect column shape displacement trajectories in the x-direction with minor drift exhibited in data for the y-direction. This is further confirmed by the Pearson correlation coefficients computed for each instrumented brick column. X-direction time-histories observed a minimum correlation factor of 0.85 with an overall average of 0.96 in comparison to the y-direction, characterised by a minimum correlation coefficient of 0.01 and average of 0.52. In some instances, the y-direction displacements did display comparable phase and frequency information with variation in amplitude. Lattice brick columns show higher correlation coefficients with smaller mean and standard deviation quantities, on average, for x- and y-directions respectively. The coefficient of variation values for lattice brick columns exhibit smaller values indicating better performance and less dispersion in comparison to the interstitial brick columns.

Interstitial brick column IB2622 exhibits a correlation coefficient of 0.96 and 0.41 on average, for x- and y-direction displacements respectively, in comparison to 0.93 and 0.15 for IB2226. LB2521 yielded Pearson correlation coefficient values of 0.98 and 0.66 whilst LB3319 generated coefficients of 0.98 and 0.86 for x- and y-direction displacements respectively. Therefore, brick column LB3319 performed best out of all comparable instrumented columns for indirect evaluation of the column shape displacements in both x- and y-directions. Results generated from the data of IB2622 yield a more accurate column shape evaluation when compared to the results for IB2226. It should be noted that correlation coefficients are much higher in each instrumented brick column in the x-direction, which corresponds to the cardinal direction of the input motion. This suggests that it is possible to accurately indirectly evaluate the column shape displacement in the direction of a ground input motion for the MLA.

The column shape evaluation for the lattice brick columns may be more accurate when compared to the interstitial columns as the LCP sensor data is not as intensively processed as the Hall Effect sensor data. Also, interface displacement LCP sensors implemented for lattice columns do not involve the comprehensive calibration procedures when compared to the interstitial hall-effect sensor tracing (Crewe et al., 2018). The sensitivity of the Hall effect sensors, however, is less certain as a result of the complex coupled sensor geometry combined with the nonlinear 6 DoF calibration performed. The LCP sensors have an approximate sensitivity of 98% resulting in a 2% error which may contribute to the more successful tracking and evaluation of indirect column shape profiles for both x- and y-directions. Errors in calibrated interface measurements could therefore be amplified up the brick column when evaluating global displacement trajectories. Although the vision system is utilised as a separate displacement monitoring system, measurements acquired cannot be considered truth data due to potential uncertainty in interpolation during tracking. At very low displacement amplitudes, the tracking

algorithm utilised by the vision system may become less accurate which could have contributed to the drift exhibited in y-displacement tracking of interstitial and lattice columns in Figure 11(b) and 12(b).

Table 1
Comparative statistical analysis of μDAQ and vision systems for performance assessment of indirect column shape displacement algorithm

MLA configuration	Pearson correlation		Mean of deviation time-history [mm]		Standard deviation of deviation time-history [mm]		Coefficient of Variation of deviation time-history	
	x	y	x	y	x	y	x	y
				IB2226				
MLA01	0.97	0.41	0.16	-0.12	0.60	0.44	3.79	3.68
MLA10	0.93	0.11	-0.02	0.04	0.46	0.32	29.65	7.92
MLA11	0.85	0.01	0.14	-0.35	0.64	0.58	4.41	-1.63
MLA13	0.95	0.07	0.22	-0.31	0.45	0.34	1.99	-1.11
				IB2622				
MLA01	0.92	0.20	0.69	-0.37	0.82	0.51	1.18	1.37
MLA10	0.94	0.17	-0.16	-0.30	0.33	0.27	-2.90	-0.90
MLA11	0.99	0.80	-0.06	-0.43	-0.16	0.25	-2.83	-0.57
MLA13	0.99	0.48	0.07	0.04	0.17	0.17	2.35	4.18
				LB2521				
MLA01	0.99	0.46	0.09	0.04	0.32	0.15	3.56	4.23
MLA10	0.97	0.78	-0.14	-0.08	0.24	0.11	-1.79	-1.28
MLA11	0.98	0.84	-0.21	-0.24	0.21	0.14	-0.96	-0.58
MLA13	0.98	0.56	-0.07	0.02	0.19	0.10	-2.67	5.25
				LB3319				
MLA01	0.97	0.78	0.06	0.07	0.33	0.23	5.57	3.19
MLA10	0.95	0.84	0.10	-0.03	0.25	0.13	2.44	-3.85
MLA11	0.99	0.87	0.05	-0.23	0.13	0.13	2.41	-0.57
MLA13	0.99	0.96	-0.05	-0.03	0.09	0.01	-1.84	-2.19

6. Conclusion

This paper provides a mathematical framework for indirectly evaluating column shape displacement profiles in an experimental quarter-sized Advanced Gas-cooled Reactor model-core like structure using direct measurements of the displacements at each brick interface for interstitial and lattice brick columns. The proposed procedure is compared against a known displacement acquired by a motion capture vision system at the top of instrumented brick columns. Qualitative analysis indicates that the computed column shape time-histories are in good agreement with measurements acquired by the vision system. Quantitative statistical analysis is carried out to evaluate the performance of the presented indirect column shape displacement algorithm for a range of MLA build configurations subject to seismic input excitation. On average, the computed standard deviations for estimated lattice brick top column, relative to the vision system measurements, are lower than interstitial column estimates. The profiles of the lattice and interstitial instrumented brick columns are in good agreement with measurements acquired separately by the motion capture vision system. Optimal performance is observed for x-direction measurements, corresponding to an overall average Pearson correlation coefficient of 0.96. The calculated y-direction displacement motions exhibit minor shifts in offset, however, the phase, frequency and amplitude are comparable showing very good agreement. This indicates that the Euler mechanics based method is appropriate in indirectly evaluating the column

shape displacement profiles for both interstitial and lattice columns. For multiple model build configurations, which represent different cracked brick scenarios, the seismic responses of the columns are shown to be significantly larger in amplitude in the presence of large numbers of cracked bricks.

Acknowledgements

The authors would like to thank EDF for financial and technical support. The views expressed in this paper are those of the authors and do not necessarily represent those of EDF.

References

Anooshehpoor, A., 2004. Methodology for Obtaining Constraints on Ground Motion from Precariously Balanced Rocks. Bulletin of the Seismological Society of America 94. https://doi.org/10.1785/0120020242

Bachmann J, Strand M, Vassiliou MF, Broccardo M, Stojadinovic B., 2019. Modelling of rocking structures: Are our models good enough?. In Online Proceedings: 2nd International Conference on Natural Hazards & Infrastructure, ICONHIC, 23-26 June 2019, Chania, Greece, pp. 970. https://doi.org/10.3929/ethz-b-000350669

Bonivento, C., Grimble, M.J., Giovanini, L., Monari, M., Paoli, A., 2008. Monitoring a gas-cooled nuclear reactor core integrity. IFAC Proceedings Volumes 41. https://doi.org/10.3182/20080706-5-KR-1001.02190

Castro, E., 2005. Investigation of degradation of AGR graphite core geometry using a whole core scale model. In: Neighbour, G. (Ed.), Proc. of the Conference on Aging Management of Graphite Reactor Cores, The Royal Society of Chemistry, Cambridge, UK., pp. 209–215.

Crewe A, Horseman T, Dietz M, Oddbjornsson O, Dihoru L, Kloukinas P, Voyagaki E, Taylor CA, 2018. Development of a high channel count distributed data acquisition system for shaking table testing. Proceedings of the 16th European Conference on Earthquake Engineering. European Association for Earthquake Engineering (EAEE), 2018.

Dasiou ME, Mouzakis HP, Psycharis IN, Papantonopoulos C, Vayas I., 2009. Experimental investigation of the seismic response of parts of ancient temples. InProc. of Prohitech conference, Protection of Historical Buildings, 21-24 June 2009, Rome, Italy

Department for Business, Energy & Industrial Strategy and Nuclear Decommissioning Authority, 2021. UK Energy in Brief 2021, National Statistics. Retrieved from https://assets.publishing.service.gov.uk/government/uploads/system/uploads/attachment_data/file/1016822/UK_Energy_in_Brief_2021.pdf

Dihoru, L., Crewe, A.J., Taylor, C.A., Horgan, T., 2011. Shaking table experimental programme. In: Neighbour, Gareth B. (Ed.), Proc. of the Conference on Modelling and Measuring Reactor Core Graphite Properties and Performance. Aston University, Cambridge, UK.

Dihoru L, Oddbjornsson O, Brasier S, Crewe AJ, Taylor CA, Steer AG, 2015. A single layer rig for exploring the dynamics of an advanced gas cooled reactor graphite core: commissioning and

proposed validation studies. InProc. of SECED Conference: Earthquake Risk and Engineering towards a Resilient World, 9–10 July 2015, Cambridge UK.

Dihoru, L., Oddbjornsson, O., Kloukinas, P., Dietz, M., Horseman, T., Voyagaki, E., Crewe, A.J., Taylor, C.A., Steer, A.G., 2017. The development of a physical model of an Advanced Gas Cooled Reactor core: Outline of the feasibility study. Nuclear Engineering and Design 323, 269–279. https://doi.org/10.1016/J.NUCENGDES.2017.01.012

Dihoru, L., Dietz, M., Horseman, T., Kloukinas, P., Oddbjornsson, O., Voyagaki, E., Crewe, A.J., Taylor, C.A., 2018. Neural networks for displacement analysis in an advanced gas cooled reactor core model. Nuclear Engineering and Design 332, 252–266. https://doi.org/10.1016/J.NUCENGDES.2018.03.039

Dihoru, L., Crewe, A.J., Horseman, T., Dietz, M., Oddbjornsson, O., Kloukinas, P., Voyagaki, E., Taylor, C.A., 2019. A computer vision approach for dynamic tracking of components in a nuclear reactor core model. Nuclear Engineering and Design 344, 1–14. https://doi.org/10.1016/J.NUCENGDES.2019.01.017

Dihoru, L., Oddbjornsson, O., Cannell, B., Crewe, A.J., Horseman, T., Dietz, M., Taylor, C.A., 2020. Experimental and computational synergy for modelling an advanced gas-cooled reactor core under seismic excitation. Earthquake Engineering & Structural Dynamics 49. https://doi.org/10.1002/eqe.3291

Dihoru, L., Oddbjornsson, O., Crewe, A.J., Taylor, C.A., 2021. Measurement techniques for column interface monitoring in an advanced gas cooled reactor model. Nuclear Engineering and Design 377, 111134. https://doi.org/10.1016/J.NUCENGDES.2021.111134

Dimitrakopoulos, E.G., DeJong, M.J., 2012a. Revisiting the rocking block: closed-form solutions and similarity laws. Proceedings of the Royal Society A: Mathematical, Physical and Engineering Sciences 468. https://doi.org/10.1098/rspa.2012.0026

Dimitrakopoulos, E.G., DeJong, M.J., 2012b. Overturning of Retrofitted Rocking Structures under Pulse-Type Excitations. Journal of Engineering Mechanics 138. https://doi.org/10.1061/(ASCE)EM.1943-7889.0000410

Flewitt, P. E. J. and Wickham, A. J. (Eds.), 2015. Engineering Challenges Associated with the Life of Graphite Reactor Cores. EMAS Publishing, ISBN 978-0-9576730-5-2.

Jones, C. J., 2005. Predicting the Stresses and Deformations of Irradiated Graphite Moderator Bricks, In: Neighbour, G. (Ed.), Proc. of the Conference on Aging Management of Graphite Reactor Cores, The Royal Society of Chemistry, Cambridge, UK., pp. 167-174.

Kralj, S.J. Humphreys and B.G.J. Duncan, 2005. Seismic modelling of an AGR core, In: Neighbour, G. (Ed.), Proc. of the Conference on Aging Management of Graphite Reactor Cores, The Royal Society of Chemistry, Cambridge, UK., pp. 193-200.

Konstantinidis, D., Makris, N., 2005. Seismic response analysis of multidrum classical columns. Earthquake Engineering & Structural Dynamics 34. https://doi.org/10.1002/eqe.478

Kounadis, A.N., 2013. Parametric study in rocking instability of a rigid block under harmonic ground pulse: A unified approach. Soil Dynamics and Earthquake Engineering 45, 125–143. https://doi.org/10.1016/J.SOILDYN.2012.10.002

McLachlan, N., Shaw, D. J. and Salih, H., 2005. Application of whole core modelling methodology to life extension of AGR reactor graphite cores. In: Neighbour, G. (Ed.), Proc. of the Conference on Aging Management of Graphite Reactor Cores, The Royal Society of Chemistry, Cambridge, UK., pp. 240-247.

Mouzakis, H.P., Psycharis, I.N., Papastamatiou, D.Y., Carydis, P.G., Papantonopoulos, C., Zambas, C., 2002. Experimental investigation of the earthquake response of a model of a marble classical column. Earthquake Engineering & Structural Dynamics 31. https://doi.org/10.1002/eqe.184

Neighbour, G.B. (Ed.), 2007. Management of Ageing in Graphite Reactor Cores. Royal Society of Chemistry, Cambridge. https://doi.org/10.1039/9781847557742

Neighbour, G.B. (Ed.), 2013. Modelling and Measuring Reactor Core Graphite Properties and Performance. RSC Publishing, Cambridge, ISBN 978-1-84973-390-8.

Oddbjornsson, O., Kloukinas, P., Gokce, T., Bourne, K., Horseman, T., Dihoru, L., Dietz, M., White, R.E., Crewe, A.J., Taylor, C.A., 2021. Design and Calibration of a Hall Effect System for Measurement of Six-Degree-of-Freedom Motion within a Stacked Column. Sensors 21. https://doi.org/10.3390/s21113740

Papantonopoulos, C., Psycharis, I.N., Papastamatiou, D.Y., Lemos, J. v., Mouzakis, H.P., 2002. Numerical prediction of the earthquake response of classical columns using the distinct element method. Earthquake Engineering & Structural Dynamics 31. https://doi.org/10.1002/eqe.185

Peña, F., Prieto, F., Lourenço, P.B., Campos Costa, A., Lemos, J. v., 2007. On the dynamics of rocking motion of single rigid-block structures. Earthquake Engineering & Structural Dynamics 36. https://doi.org/10.1002/eqe.739

Psycharis, I.N., Papastamatiou, D.Y., Alexandris, A.P., 2000. Parametric investigation of the stability of classical columns under harmonic and earthquake excitations. Earthquake Engineering & Structural Dynamics 29. https://doi.org/10.1002/1096-9845(200008)29:8<1093::AID-EQE953>3.0.CO;2-S

Psycharis, I.N., Lemos, J. v., Papastamatiou, D.Y., Zambas, C., Papantonopoulos, C., 2003. Numerical study of the seismic behaviour of a part of the Parthenon Pronaos. Earthquake Engineering & Structural Dynamics 32. https://doi.org/10.1002/eqe.315

Psycharis, I.N., Fragiadakis, M., Stefanou, I., 2013. Seismic reliability assessment of classical columns subjected to near-fault ground motions. Earthquake Engineering & Structural Dynamics. https://doi.org/10.1002/eqe.2312

Reggiani Manzo, N., Vassiliou, M.F., 2019. Displacement‐based analysis and design of rocking structures. Earthquake Engineering & Structural Dynamics 48. https://doi.org/10.1002/eqe.3217

Reggiani Manzo, N., Vassiliou, M.F., 2021. Simplified analysis of bilinear elastic systems exhibiting negative stiffness behavior. Earthquake Engineering & Structural Dynamics 50. https://doi.org/10.1002/eqe.3347

Rogers, S., 2012. Graphite Core PLEX, 81-Brick Array Solfec Comparison (Atkins Report Ref. No. 5101060/23/06/01, 19/01/2012).

Vassiliou, M.F., Broccardo, M., Cengiz, C., Dietz, M., Dihoru, L., Gunay, S., Mosalam, K.M., Mylonakis, G., Sextos, A., Stojadinovic, B., 2021. Shake table testing of a rocking podium: Results of a blind prediction contest. Earthquake Engineering & Structural Dynamics 50. https://doi.org/10.1002/eqe.3386

Voyagaki, E., Psycharis, I.N., Mylonakis, G., 2013. Rocking response and overturning criteria for free standing rigid blocks to single—lobe pulses. Soil Dynamics and Earthquake Engineering 46, 85–95. https://doi.org/10.1016/J.SOILDYN.2012.11.010

Voyagaki, E., Psycharis, I.N., Mylonakis, G., 2014. Complex Response of a Rocking Block to a Full-Cycle Pulse. Journal of Engineering Mechanics 140. https://doi.org/10.1061/(ASCE)EM.1943-7889.0000712

Voyagaki E, Vamvatsikos D., 2015. Probabilistic assessment of rocking response for simply-supported rigid blocks. InProc. of SECED Conference: Earthquake Risk and Engineering towards a Resilient World, 9–10 July 2015, Cambridge UK.

Voyagaki, E., Kloukinas, P., Dietz, M., Dihoru, L., Horseman, T., Oddbjornsson, O., Crewe, A.J., Taylor, C.A., Steer, A., 2018. Earthquake response of a multiblock nuclear reactor graphite core: Experimental model vs simulations. Earthquake Engineering & Structural Dynamics 47. https://doi.org/10.1002/eqe.3100

Young, A., Berry, C., West, G.M., McArthur, S.D.J., 2019. A generalized model for fuel channel bore estimation in AGR cores. Nuclear Engineering and Design 352, 110158. https://doi.org/10.1016/J.NUCENGDES.2019.110158

Zhang, J., Makris, N., 2001. Rocking Response of Free-Standing Blocks under Cycloidal Pulses. Journal of Engineering Mechanics 127. https://doi.org/10.1061/(ASCE)0733-9399(2001)127:5(473)